



Article

A Model Combining Sensitive Vegetation Indices and Fractional-Order Differential Characteristic Bands for SPAD Value Estimation in Cd-Contaminated Rice Leaves

Rongcai Tian ¹, Bin Zou ^{1,2}, Shenxin Li ^{1,*} , Li Dai ³ , Bo Zhang ¹, Yulong Wang ¹, Hao Tu ¹, Jie Zhang ¹ and Lunwen Zou ⁴

¹ School of Geosciences and Info-Physics, Central South University, Changsha 410083, China; 215001013@csu.edu.cn (R.T.); 210010@csu.edu.cn (B.Z.); 225001021@csu.edu.cn (B.Z.); 205001031@csu.edu.cn (Y.W.); biuuuu@csu.edu.cn (H.T.); 235012171@csu.edu.cn (J.Z.)

² Key Laboratory of Metallogenic Prediction of Nonferrous Metals and Geological Environment Monitoring of Chinese Ministry of Education, Changsha 410083, China

³ Hunan Rice Research Institute, Changsha 410125, China; daili@hunaas.cn

⁴ School of Geographical Sciences, Hunan Normal University, Changsha 410081, China; 201940450162@hunnu.edu.cn

* Correspondence: shenxin823@csu.edu.cn

Abstract: Rapid and nondestructive estimation of leaf SPAD values is crucial for monitoring the effects of cadmium (Cd) stress in rice. To address the issue of low estimation accuracy in leaf SPAD value models due to the loss of spectral information in existing studies, a new estimation model, which combines sensitive vegetation indices (VIss) and fractional order differential characteristic bands (FODcb), is proposed in this study. To validate the effectiveness of this new model, three scenarios, with no Cd contamination, 1.0 mg/kg Cd contamination, and 1.4 mg/kg Cd contamination, were set up. Leaf spectral reflectance and SPAD values were measured during the critical growth period of rice. Subsequently, 16 vegetation indices were constructed, and fractional order difference (FOD) transformation was applied to process the spectral data. The variable importance in projection (VIP) algorithm was employed to extract VIss and FODcb. Finally, the random forest (RF) algorithm was used to construct three models, VIss + FODcb-RF, FODcb-RF, and VIss-RF. The estimated leaf SPAD values for the three models showed that: (1) there was a significant difference between the leaf SPAD values with no Cd contamination and those treated with 1.4 mg/kg Cd contamination on the 31st and 87th days after transplanting; (2) the 400–773 nm spectral range was sensitive for estimating leaf SPAD values, with the Cd-contaminated scenario exhibiting higher reflectance in the visible wavelength range than the Cd-uncontaminated scenario; (3) compared with the individual FODcb-RF and VIss-RF models, the combined model (VIss + FODcb-RF) improved the estimation accuracy of the leaf SPAD values. Particularly, the VIss + FOD_{1.2cb}-RF model provided the best performance, with R²_v, RMSE_v, and RPD_v values of 0.821, 2.621, and 2.296, respectively. In conclusion, this study demonstrates the effectiveness of combining VIss and FODcb for accurately estimating Cd-contaminated rice leaf SPAD values. This finding will provide a methodological reference for remote sensing monitoring of Cd contamination in rice.

Keywords: Cd-contaminated rice; leaf SPAD values; vegetation indices; fractional order differential characteristic bands; hyperspectral remote sensing



Academic Editor: Roberto Alves Braga Júnior

Received: 18 December 2024

Revised: 4 January 2025

Accepted: 28 January 2025

Published: 31 January 2025

Citation: Tian, R.; Zou, B.; Li, S.; Dai, L.; Zhang, B.; Wang, Y.; Tu, H.; Zhang, J.; Zou, L. A Model Combining Sensitive Vegetation Indices and Fractional-Order Differential Characteristic Bands for SPAD Value Estimation in Cd-Contaminated Rice Leaves. *Agriculture* **2025**, *15*, 311. <https://doi.org/10.3390/agriculture15030311>

Copyright: © 2025 by the authors. Licensee MDPI, Basel, Switzerland. This article is an open access article distributed under the terms and conditions of the Creative Commons Attribution (CC BY) license (<https://creativecommons.org/licenses/by/4.0/>).

1. Introduction

Cadmium (Cd)-contaminated rice not only poses a threat to human health but constitutes a potential risk to national and global food security [1–3]. Thus, strengthening the regulation of the growth process of Cd-accumulating rice is critical to ensuring its quality and safety. Chlorophyll content is a reliable indicator of crop nutritional status, photosynthetic capacity, and developmental stage and is also a crucial parameter for assessing crop health and the extent of environmental stress [4–6]. In addition, chlorophyll content effectively reflects the extent of Cd contamination and can serve as a response indicator [7,8]. Consequently, it has emerged as one of the most important metrics for monitoring Cd contamination in rice. Numerous studies [9–11] have shown a significant correlation between leaf soil and plant analyzer development (SPAD) values and measured chlorophyll content, making the former widely used to characterize chlorophyll content. However, direct field measurement of leaf SPAD values using specialized instruments remains labor-intensive, time-consuming, and challenging to implement on a large scale. Therefore, the development of rapid and accurate methods for monitoring leaf SPAD values is crucial for effectively monitoring Cd contamination in rice crops.

Hyperspectral remote sensing is characterized by high spectral resolution, multiple continuous bands, and rich information. In recent years, research on leaf SPAD values using remote sensing under adverse conditions has gradually increased. Numerous studies have utilized hyperspectral remote sensing technology to estimate leaf SPAD values in crops such as maize [12–15], cotton [16], and rice [17] under stress conditions such as drought, salinity, disease, and pest infestations. The predicted R^2 values ranged from 0.61 to 0.91, demonstrating the feasibility of using leaf SPAD values for crop stress monitoring. However, it is evident that current research has not sufficiently addressed crop heavy metal stress. The root cause lies in the fact that heavy metals are trace elements present in very low concentrations within crops and that their spectral response mechanisms remain poorly understood. For these reasons, research on crop heavy metal stress has primarily focused on qualitative analyses of the physiological, biochemical, and spectral response levels under heavy metal stress [18–21], which makes it difficult to precisely quantify the quantitative relationship between biochemical parameters and spectral reflectance. Although only a few studies have started to explore quantitative spectral estimation models for lettuce leaf SPAD values under different Cd concentration stresses [22], it has been found that leaf SPAD estimation based on the red-edge normalized index was optimal, with a coefficient of determination (R^2) of 0.78. However, most of the vegetation indices used in modeling are borrowed from other fields, which may make them less relevant to leaf SPAD values under heavy metal stress. Furthermore, since vegetation indices are typically constructed from reflectance data corresponding to two or three bands, they may fail to capture all the spectral information related to leaf SPAD values. As a result, the loss of spectral information could be a key limiting factor in improving model accuracy further. Furthermore, previous studies [23–25] have shown that bands at 400–570 nm, 940–990 nm, and 1000 nm are characteristic of the spectral response of Cd-contaminated soils. However, these bands are often excluded in the construction of the vegetation indices. Therefore, it remains to be determined whether including these characteristic bands in the estimation of SPAD values for Cd-contaminated rice leaves can improve estimation accuracy.

The selection of characteristic bands is crucial for establishing a high-precision estimation model. Effective preprocessing of spectral data is an essential prerequisite for this selection. The fractional-order differential (FOD) preprocessing method can highlight subtle changes in spectral information, enhance weaker spectral features, and improve the signal-to-noise ratio of spectral reflectance. It has been widely applied in remote sensing inversions of rice heavy metal content [26], soil organic matter content [27–31], heavy metal

content [32,33], and salt content [34–36]. This approach may help to extract weak signals in the rice spectral response under Cd stress. However, the FOD-transformed spectral data often encounter the curse of dimensionality, and the direct use of full-spectrum spectral data to construct an estimation model is computationally expensive, inefficient, and unsuitable for generalized applications. Thus, combining vegetation indices (VIs) and fractional-order differential characteristic bands (FODcb) is an important issue that needs to be addressed in order to achieve high-precision and high-efficiency estimation of SPAD values in rice leaves under the weak remote sensing signals from Cd contamination.

Additionally, because of the unique advantages of the random forest (RF) model in terms of modelling variable importance interpretation and handling small sample sizes [25,37], this study utilized FOD to process the spectral reflectance data of rice under Cd contamination conditions and incorporated FODcb into VIss to estimate the rice leaf SPAD values using RF modeling. The objectives of this study are threefold: (1) to propose a novel model combining VIss and FODcb and verify its validity in estimating the SPAD values of Cd-contaminated rice leaves; (2) to reveal the response patterns of SPAD values and spectral reflectance in rice leaves under Cd stress, thereby providing a theoretical basis for model construction; and (3) to identify the characteristic bands that should be emphasized in the application of the combined model.

2. Materials and Methods

2.1. Experimental Design

The experiment was conducted in 2022 at the test base of the Hunan Rice Research Institute in Chunhua Town, Changsha County, Hunan Province. To minimize the influence of external environmental factors, this study designed an innovative Cd pool experiment with a rail-type plastic trellis that automatically retracts during rainy periods. To better align with the real growing conditions of rice, this study followed the criteria outlined in the “Soil Pollution Risk Control Standards for Agricultural Land” (GB15618-2018) for categorizing soil environmental quality [38]. It also considered the Cd contamination situation in rice fields in Hunan Province. Three Cd contamination scenarios were set up with different ratios of actual Cd-contaminated soil quality, namely, no Cd contamination (NC), 1.0 mg/kg Cd contamination (C1), and 1.4 mg/kg Cd contamination (C2). Twelve low-Cd-accumulating breeding materials, one-season late rice varieties obtained through radiation mutagenesis, were selected for testing. Rice seeds were sown on 17 May, transplanted on 20 June, and harvested on 21 September, with a total growth period of 128 days in the field. For each Cd contamination scenario, twelve low-Cd-accumulating rice materials were planted, with three replications. The experiment setup and treatment scheme are shown schematically in Figure 1.

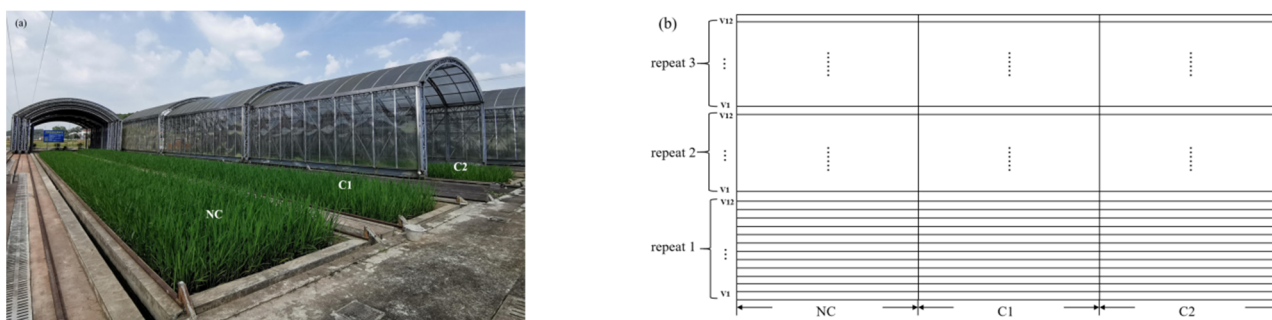


Figure 1. Experimental diagrams: (a) experimenting with actual scenarios and (b) schematic diagram of the pilot treatment program (where V1–V12 denote the 12 low-Cd-accumulating rice test materials and repeat 1, repeat 2, and repeat 3 represent three replications of the same Cd-contaminated rice test material).

2.2. Workflow

The flowchart of this study is depicted in Figure 2. To determine the optimal model for estimating SPAD values in Cd-contaminated rice leaves, we constructed and compared an RF model based on the combination of VI_{ss} and FOD_{cb}, as well as models based on FOD_{cb} and VI_{ss} alone. This study included the following four steps. (1) Data acquisition: spectral reflectance data of rice leaves and corresponding SPAD values were collected on days 31, 46, 66, and 87 after rice transplantation. (2) Data processing: The Kennard–Stone (KS) algorithm was used to divide the dataset into a calibration set and a validation set. Sixteen vegetation indices commonly used for estimating chlorophyll content were constructed, and the original spectral data were processed with FOD. (3) Feature selection: The variable importance in projection (VIP) algorithm was employed to select VI_{ss} and FOD_{cb}. (4) Modelling and validation: Three strategies (based on the combination of VI_{ss} with FOD_{cb} and on FOD_{cb} and VI_{ss} alone) were utilized to construct SPAD value estimation models, which were then validated using external independent samples.

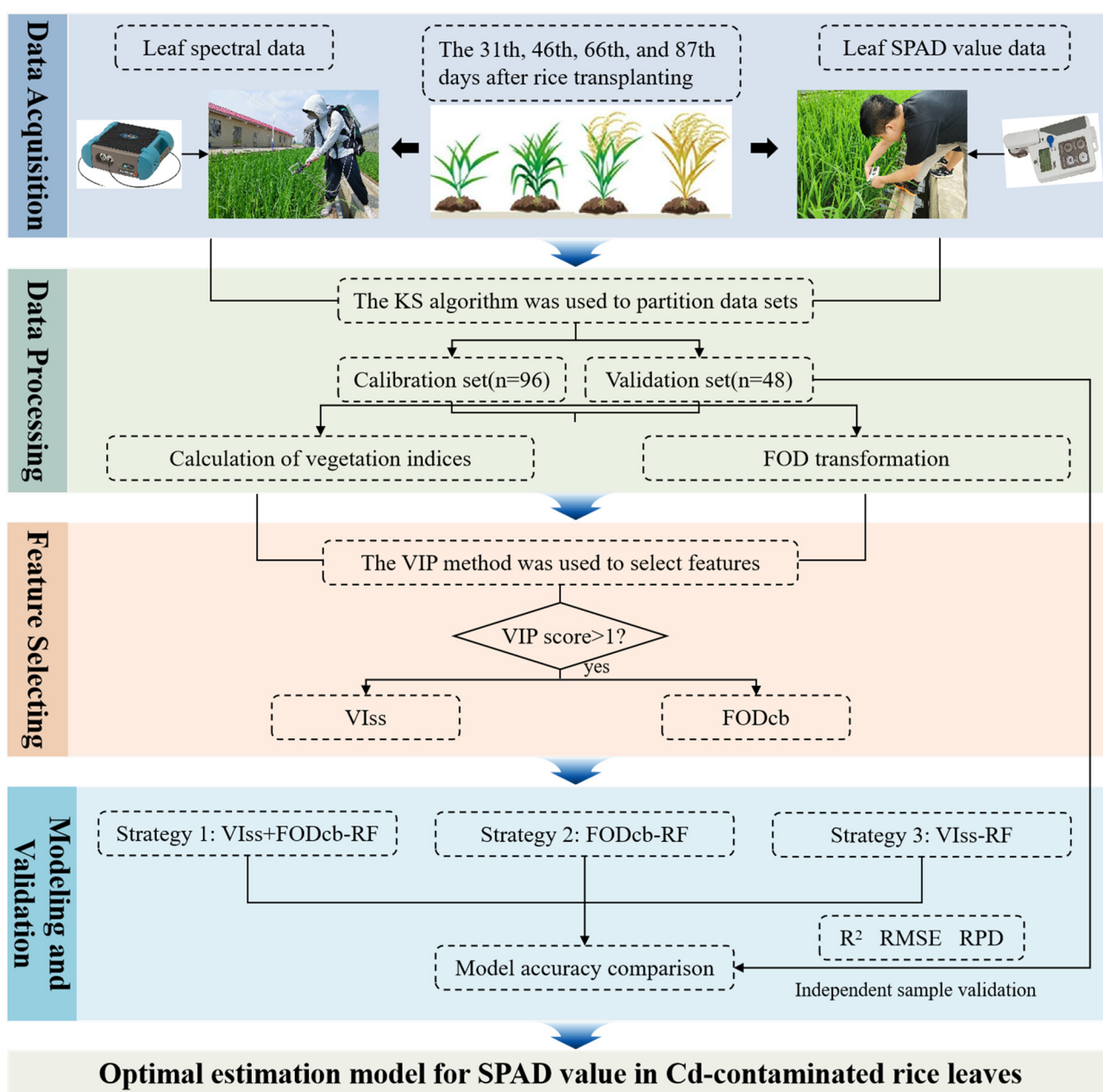


Figure 2. Flowchart of this study.

2.3. Data Acquisition

Hyperspectral and SPAD data of the flag leaf were collected at 14-day intervals following the transplantation of rice materials in each experiment. However, because of weather conditions, variations in leaf size, and other factors, the planned data collection schedule could not be strictly adhered to. Adjustments were made based on the actual measurement time. As a result, data were collected on four occasions, specifically on the 31st, 46th, 66th, and 87th days after rice transplantation.

2.3.1. Measurement of Leaf Spectral Reflectance

Canopy hyperspectral data are easily affected by the soil background and weather conditions, making it difficult to ensure data accuracy. However, leaf hyperspectral data can be measured *in vivo* with the help of the built-in active light source of the instrument, which effectively reduces interference from the external environment and increases data accuracy. For this reason, rice flag leaf hyperspectral data were collected at the 31st, 46th, 66th, and 87th days after transplanting each material using a FieldSpec4 ground spectrometer (manufactured by Analytical Spectra Device, ASD, Boulder, CO, USA). The instrument was equipped with an active light source and a handheld leaf spectrum probe, which allowed direct *in vivo* measure of the leaf. The instrument had a wavelength range of 350–2500 nm, with a spectral sampling interval of 1.4 nm for 350–1000 nm and 1.1 nm for 1001–2500 nm, as well as spectral resolutions of 3 nm@700 nm and 8 nm@1400 nm/2100 nm. For each rice material, two flag leaves with uniform growth were selected for leaf spectroscopy, with 10 replications performed. Before measuring each rice material, calibration was performed once using the standard whiteboard that came with the handheld leaf spectroscopy probe. After calibration, the whiteboard was replaced with a blackboard for leaf spectrometry.

2.3.2. Measurement of Leaf SPAD Values

The flag leaf plays a pivotal role in photosynthesis in rice and is widely recognized as the primary source of assimilates contributing to both yield and quality [39,40]. As such, monitoring the flag leaf provides valuable insights into the growth status of rice plants. In this study, the SPAD-502 chlorophyll meter (Konica Minolta, Tokyo, Japan) was utilized to quantify the SPAD values of flag leaves from various rice materials subjected to different level of Cd contamination. Specifically, two flag leaves exhibiting relatively uniform growth were randomly selected from each row of experimental material. Each selected leaf was divided into three distinct sections: the tip, middle, and base. SPAD measurements were then recorded for each of these sections, ensuring that the adaxial side of the leaf was consistently positioned towards the emission window of the SPAD-502 m, while avoiding the primary veins. The average SPAD value from the three sections was computed as the representative value for each leaf. The overall SPAD value for each experimental material was determined as the mean of the readings from the two selected leaves. To reduce the potential influence of edge effects, leaves from rice plants located at the borders of each row were excluded.

2.4. Data Processing

2.4.1. Spectral Preprocessing and Dataset Partitioning

There is significant noise in the 350–400 nm spectral band due to the quantum and lattice effects of the sensor material itself. Previous studies have shown that the visible spectrum, along with part of the near-infrared spectrum (400–1000 nm), is commonly employed for evaluating various parameters related to the growth, development, and nutritional status of rice [41–44]. Furthermore, the near-infrared spectral range beyond 1000 nm is typically employed for estimating crop quality parameters, such as protein and starch

content [45–47]. Therefore, the spectral range from 400 to 1000 nm was selected for this study. The KS algorithm [48,49] is based on Euclidean distance calculation, which ensures that the samples in the training set are evenly distributed in terms of spatial distance, thus making the dataset division representative. This algorithm is one of the most commonly used methods for sample set division. In this study, the KS algorithm was used to divide the dataset at 2:1 ratio. The results are shown in Table 1. As shown in Table 1, the SPAD values of the calibration set ranged from 8.700 to 48.600, with a mean and coefficient of variation of 34.547 ± 9.724 and 28.1%, respectively. The SPAD values of the validation set ranged from 17.000 to 47.200, with a mean and coefficient of variation of 39.079 ± 6.253 and 16.0%, respectively. Statistical analysis of the calibration and validation sets revealed that the SPAD values of the validation set were within the range of the calibration set. This indicates that the division of the calibration and validation sets was reasonable and that the validation samples could be used to independently validate the model’s accuracy.

Table 1. Sample set division of leaf SPAD values.

Sample Set	Size	Max.	Min.	Mean	SD	CV (%)
Calibration set	96	48.600	8.700	34.547	9.724	28.1
Validation set	48	47.200	17.000	39.079	6.253	16.0
Total	144	48.600	8.700	36.058	8.928	24.8

2.4.2. Vegetation Index Calculation

Vegetation indices are numerical indicators that represent the condition of vegetation and are calculated through remote sensing data. These indices are commonly used to evaluate and monitor various aspects of vegetation, including growth, health status, and photosynthetic efficiency. Based on the spectral response characteristics of the chlorophyll content and previous research findings, a total of 16 commonly used vegetation indices for estimating SPAD values were selected for this study. The specific calculation formulas are provided in Table 2.

Table 2. Calculation formulas for vegetation indices.

Generic Name (Abbreviation)	Formula	Reference
Normalized Difference Vegetation Index (NDVI)	$(R800 - R680)/(R800 + R680)$	[50]
Difference Vegetation Index (DVI)	$R800 - R680$	[50,51]
Simple Ratio Index (SRI)	$R800/R680$	[52]
Enhanced Vegetation Index (EVI)	$2.5 \times (R800 - R680)/(R800 + 6 \times R680 - 7.5 \times R450 + 1)$	[53]
Photochemical Reflectance Index (PRI)	$(R550 - R530)/(R550 + R530)$	[54]
Normalized Phaeophytinization Index (NPQI)	$(R415 - R435)/(R415 + R435)$	[55]
Structure Insensitive Pigment Index (SIPI)	$(R800 - R445)/(R800 + R680)$	[56]
Modified Chlorophyll Absorption in Reflectance Index (MCARI)	$[(R700 - R670) - 0.2 \times (R700 - R550)] \times (R700/R670)$	[57]
Transformed Chlorophyll Absorption in Reflectance Index (TCARI)	$3 \times [(R700 - R670) - 0.2 \times (R700 - R550)] \times (R700/R670)$	[58]
NVI (R640,R732,R752)	$(R752 - R732)/(R732 - R640)$	[59]
Carotenoid/Chlorophyll Ratio Index (CCRI)	$[(R720 - R521) \times R705]/[(R750 - R705) \times R521]$	[50]
Red-edge Chlorophyll Index (CI _{re})	$[R760 - R800]/[R690 - R720] - 1$	[60]
Normalized Red-Edge Differences (NDRE)	$(R783 - R705)/(R783 + R705)$	[61]
Normalized Pigment Chlorophyll Index (NPCI)	$(R680 - R430)/(R680 + R430)$	[51]
Modified Red-Edge Normalized Difference Vegetation Index (mND705)	$(R750 - R705)/(R750 + R705 - 2 \times R445)$	[52]
Heavy Metal Cd Stress-Sensitive Spectral Index (HCSI)	$((R780 - R712)/R678)(R678/R550)$	[8]

2.4.3. FOD Transforming

FOD was first proposed by l'Hôpital in 1695. It alters the slope and curvature of the spectral curve by refining the order [62], thereby amplifying weak differences in the characteristic bands between the spectral curves under different fractional orders. This allows it to highlight subtle changes in the data and overall information more effectively than integer-order differentiation. FOD has been applied to enhance weak information in the study of rice Cd and lead (Pb) [26], among others. In this study, the Grünwald–Letnikov (G-L) algorithm, which is based on the definition of integer-order differentiation, was used to calculate the spectral reflectance of rice leaves under Cd stress using FOD. The calculation equation is as follows:

$$\frac{d^v f(\lambda)}{d\lambda^v} \approx f(\lambda) + (-v)f(\lambda - 1) + \frac{(-v)(-v+1)}{2}f(\lambda - 2) + \dots + \frac{\Gamma(-v+1)}{n!\Gamma(-v+n+1)}f(\lambda - n) \quad (1)$$

where n is the difference between the upper and lower derivatives, $f(\lambda)$ is a function with the reflectance at wavelength λ as the independent variable, Γ is the gamma function, and v is the order. The fractional order in this study ranged from 0 to 2 orders, with a step size of 0.2 orders and a total of 11 orders.

2.5. Feature Selecting

The VIP method, which is a variable selection technique based on partial least squares regression (PLSR), was used to select VI_{ss} and FOD_{cb}. The main idea behind the VIP method is to cumulatively calculate the importance of each variable j influenced by the component w . This is done by calculating the VIP score of each variable in the PLSR model, which enables the selection of spectral bands [23]. Since the squared mean of the VIP scores equals 1, $VIP > 1$ is commonly used as the selection criterion. The VIP scores can be calculated based on the optimal PLSR model using the following formula [63]:

$$VIP_j = \sqrt{\frac{p \sum_{k=1}^h \left(SS(b_k t_k) (w_{jk} / \|w_k\|)^2 \right)}{\sum_{k=1}^h SS(b_k t_k)}} \quad (2)$$

where $SS(b_k t_k) = b_k^2 t_k^t t_k$ denotes the explained sum of squares of the K th component, w is the weight matrix, and h is the number of latent variables in the optimal PLSR model.

2.6. Modelling and Validation

2.6.1. Random Forest Modelling

The RF algorithm is an ensemble learning method based on decision trees that uses the bootstrap resampling method with put-back sampling and calculates the results of multiple tree predictions based on the principle of weighted averaging [64,65]. This algorithm offers advantages such as versatility, fast training speed, high efficiency, and robustness to noise [66,67], and has been widely used in the inverse modelling of crop physical and chemical parameters [68–70]. In this study, the RF regression model was established using the categorical regression tree as the basic unit. In the RF regression model, the selected VI_{ss}, FOD_{cb}, and their combination obtained through the VIP method were used as independent variables, while the SPAD values were used as the dependent variable. The model input parameters were optimized using the Bayesian grid search method, with the goal of minimizing the root mean squared error (RMSE) of the model output to obtain the optimal parameter values. The optimal solutions for the three categories of model input parameters are presented in Table 3. The RF modelling process was implemented in the Python 3.10.12 environment.

Table 3. Optimal input parameters of the random forest corresponding to each model.

Model Types		Optimal Input Parameters					
		n_estimators	max_depth	max_leaf_nodes	max_features	min_samples_split	min_samples_leaf
sensitive vegetation indices	VI _{SS}	413	16	25	0.5	13	22
	FOD _{0cb}	1006	10	7	Log2	18	19
fractional-order differential characteristic bands	FOD _{0.2cb}	467	4	24	5	20	19
	FOD _{0.4cb}	412	20	17	5	22	19
	FOD _{0.6cb}	923	4	5	0.5	19	19
	FOD _{0.8cb}	183	31	4	5	22	19
	FOD _{1.0cb}	178	23	19	Log2	21	15
	FOD _{1.2cb}	541	23	30	0.5	11	7
	FOD _{1.4cb}	933	23	27	None	17	4
	FOD _{1.6cb}	111	21	4	0.5	16	18
	FOD _{1.8cb}	123	8	29	5	25	18
	FOD _{2.0cb}	962	2	3	0.8	19	22
combination of the sensitive vegetation indices and fractional-order differential characteristic bands	VI _{SS} + FOD _{0cb}	547	27	6	None	31	19
	VI _{SS} + FOD _{0.2cb}	511	18	3	0.8	28	19
	VI _{SS} + FOD _{0.4cb}	1100	5	28	0.8	21	19
	VI _{SS} + FOD _{0.6cb}	819	12	8	None	13	18
	VI _{SS} + FOD _{0.8cb}	712	17	5	0.5	7	19
	VI _{SS} + FOD _{1.0cb}	762	30	31	sqrt	5	19
	VI _{SS} + FOD _{1.2cb}	106	14	32	None	8	1
	VI _{SS} + FOD _{1.4cb}	517	30	8	None	2	1
	VI _{SS} + FOD _{1.6cb}	538	30	7	0.8	18	18
	VI _{SS} + FOD _{1.8cb}	830	3	24	0.2	15	18
VI _{SS} + FOD _{2.0cb}	208	28	15	5	9	20	

2.6.2. Model Accuracy Evaluation

Model accuracy was evaluated using R^2 , RMSE, and relative percent deviation (RPD) [71,72]. A reliable model should exhibit high R^2 , low RMSE, and high RPD values. When R^2 is closer to 1 and the RMSE is smaller, it indicates a better model fit and higher prediction accuracy. When $RPD < 1.4$, the model is considered incapable of making predictions; when $1.4 \leq RPD < 2$, the model can provide rough estimates; and when $RPD \geq 2$, the model is considered to have superior predictive ability [73,74]. The formulas for R^2 , RMSE, and RPD are as follows:

$$R^2 = 1 - \frac{\sum_{i=1}^n (y_i - \hat{y}_i)^2}{\sum_{i=1}^n (y_i - \bar{y})^2} \tag{3}$$

$$RMSE = \sqrt{\frac{\sum_{i=1}^n (y_i - \hat{y}_i)^2}{n}} \tag{4}$$

$$RPD = \frac{Std_v}{RMSE_v} \tag{5}$$

where y_i denotes the SPAD measured value, \hat{y}_i denotes the SPAD predicted value, \bar{y} denotes the SPAD mean value, n denotes the number of samples, Std_v denotes the standard error of the validation set, and $RMSE_v$ denotes the root mean square error of the validation set.

3. Results

3.1. SPAD Value Changed Under Different Cd Contamination Scenarios

Figure 3 shows the trends of SPAD values of rice leaves under different Cd contamination scenarios on the 31st, 46th, 66th, and 87th days after transplanting. As shown in the figure, the overall trend of the SPAD values of the rice leaves under different Cd contamination scenarios was consistent by the 87th day after transplanting: the SPAD values generally decreased with the progression of the reproductive process, except for the plants in the no Cd contamination scenario, which showed a rebound in SPAD values on the 66th day. From the perspective of the different Cd contamination scenarios, on the 31st day after transplanting, the SPAD values of leaves in the 1.4 mg/kg Cd contam-

ination scenario were higher than those in the no Cd contamination and 1.0 mg/kg Cd contamination scenarios. This could be attributed to the fact that, at this stage, the rice was in the peak period of nutrient growth and had the ability to self-repair because of the low concentration of Cd contamination. However, the opposite trend in SPAD values was observed on the 66th and 87th days after transplanting, showing the following order: no Cd contamination > Cd contamination. This could be due to the fact that, during the late stage of rice growth, leaf growth slowed down, and the presence of Cd contamination led to a decrease in the structure of chloroplasts, reduced chlorophyllase activity, and decreased synthesis of photosynthetic pigments, ultimately resulting in a decrease in SPAD values. Moreover, according to the analysis of significant differences, we also found that the leaf SPAD values under the no Cd contamination and 1.4 mg/kg Cd contamination scenarios were significantly different on the 31st and 87th days after transplanting. This finding provides a theoretical basis for using SPAD values to indirectly monitor Cd stress in rice.

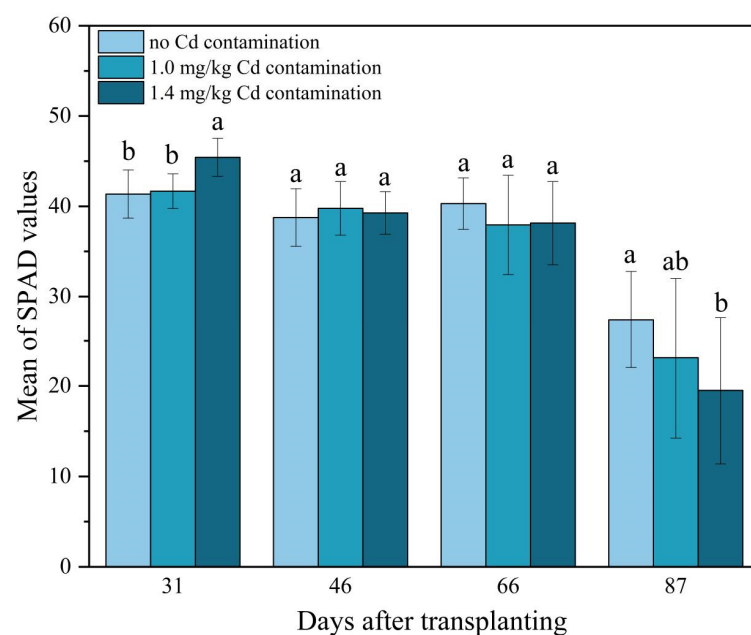


Figure 3. Changes in SPAD values of rice leaves with time under different Cd contamination scenarios (where same lowercase letters in the figure indicate no significant differences between scenarios, while different lowercase letters indicate significant differences between scenarios).

3.2. Characteristic Bands Indicated SPAD Values and Their Changes

The selection of spectral response characteristic bands for SPAD values was carried out according to the rule that VIP scores should be greater than 1. The results of the spectral response characteristic bands for Cd-contaminated rice leaves of different orders are shown in Table 4. Table 4 shows that the number of characteristic bands varied with different FOD transformations. Overall, there was a trend of first decreasing, then increasing, and then again decreasing in the number of characteristic bands as the order increased. Specifically, the number of characteristic bands decreased with increasing order in the range of 0–1.0, increased slightly with increasing order in the range of 1.0–1.6, and then decreased again. In addition, the specific positions of the characteristic bands exhibited decreasing continuity with increasing fractional order. Specifically, the continuity was stronger in the 0–0.8 order characteristic band positions, while the positions of the 1.0–2.0 order characteristic bands gradually became more dispersed. In summary, the characteristic bands for the SPAD values of Cd-contaminated rice leaves were roughly located in the wavelength range of 400–773 nm.

Table 4. Spectral response characteristic bands of leaf SPAD values at different fractional orders.

Fractional Order	Number of Characteristic Bands	Characteristic Bands (nm)
FOD _{0cb}	314	405–718
FOD _{0.2cb}	306	400–705
FOD _{0.4cb}	303	400–702
FOD _{0.6cb}	299	400, 403–700
FOD _{0.8cb}	281	407–408, 415–418, 420–700
FOD _{1.0cb}	248	411, 443–444, 449, 451–452, 463, 482–564, 601–626, 634–675, 678–698, 705–773
FOD _{1.2cb}	261	444–445, 447, 451–492, 508–677, 680–688, 695–731
FOD _{1.4cb}	271	443–444, 446, 450–452, 454–676, 679–685, 692–726
FOD _{1.6cb}	275	433, 437, 441, 443–444, 446, 450–452, 454–477, 479–676, 679–684, 689–726
FOD _{1.8cb}	262	434, 438, 447, 452, 455–456, 458–459, 462–468, 470–478, 480–485, 487–677, 680–683, 688–724 481, 487, 5494–495, 501, 515–516, 518–519, 522–523, 548, 564–566, 569–570, 597–598, 600–606, 608–609, 616, 618–623, 625–626, 631–644, 647–648, 650, 652–659, 662–688, 691–715, 717–718, 724–757, 759–760, 763, 768, 781, 972, 980, 992
FOD _{2.0cb}	158	

Figure 4 shows the spectral reflectance of rice leaves after FOD under different Cd contamination scenarios. From the original spectral reflectance in Figure 4a, it can be observed that rice leaves under Cd contamination displayed spectral characteristics typical of green plants. In the visible light range, because of the influence of pigments, chlorophyll strongly absorbs blue and red light while weakly absorbing green light, exhibiting the characteristic “blue valley”, “red valley”, and “green peak” of green plants. In the near-infrared range, with minimal absorption due to the influence of the leaf cell structure, the reflectance increases, forming a “near-infrared plateau”. Furthermore, because of the combined effect of the “red valley” and “near-infrared plateau”, the reflectance spectrum sharply increases from the red light band to the near-infrared band, forming the characteristic “red edge” of green plants. By analyzing the spectral reflectance under different Cd contamination scenarios, differences in certain bands were observed. Specifically, within the visible light spectrum, the spectral reflectance of Cd-contaminated leaves was greater than that of rice leaves without Cd contamination. In the near-infrared range, the spectral reflectance of leaves under the 1.4 mg/kg Cd contamination scenario decreased compared with that under the no Cd contamination scenario, while the opposite trend was observed under the 1.0 mg/kg Cd contamination scenario. Figure 4b–k show the results of FOD processing of the original spectra. The spectral reflectance decreased with increasing order and gradually converged to zero. The changes in the spectral reflectance of Cd-contaminated rice leaves indicate that rice leaves exhibit a spectral response to Cd stress, which lays a theoretical foundation for remote sensing monitoring of Cd-contaminated rice.

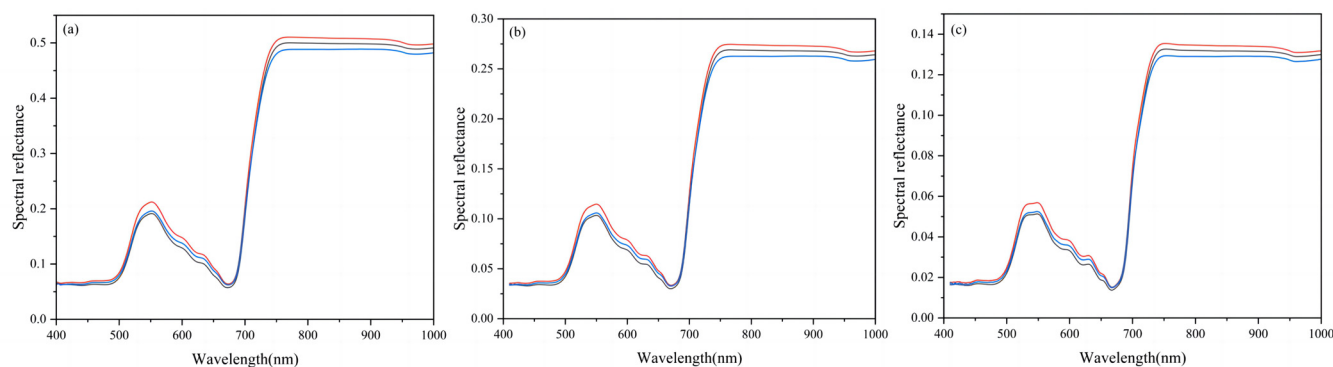


Figure 4. Cont.

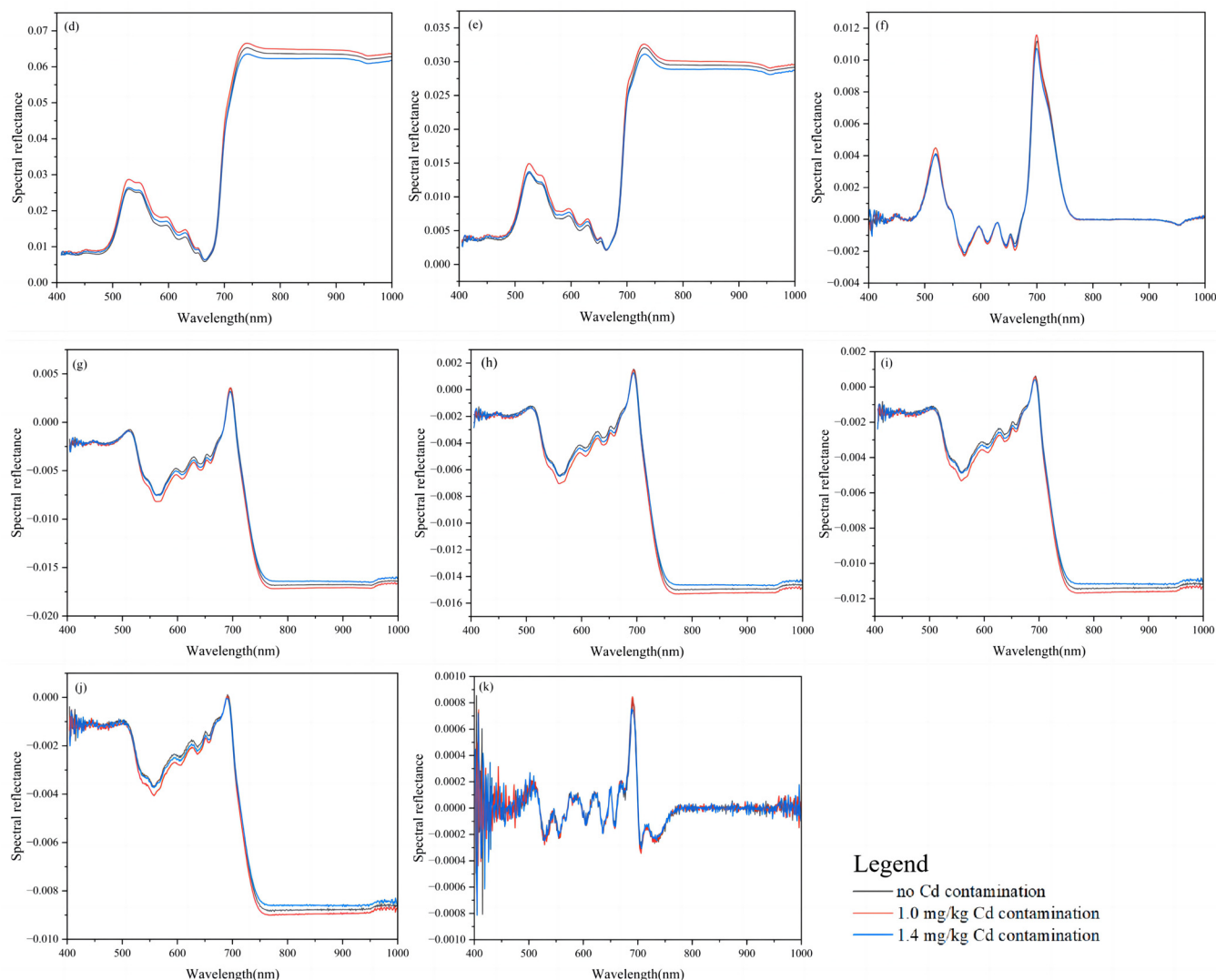


Figure 4. Spectral reflectance of leaves under different Cd contamination scenarios under FOD (where (a–k) denote the 0th order, 0.2nd order, 0.4th order, 0.6th order, 0.8th order, 1.0th order, 1.2nd order, 1.4th order, 1.6th order, 1.8th order, and 2.0th order differential transformations, respectively).

3.3. Estimation Accuracy of SPAD Values with the VI_{ss} + FOD_{cb} Model

Sensitivity analysis of 16 vegetation indices using the VIP algorithm identified a total of 8 sensitive vegetation indices: HCSI, SIPI, NDRE, NDVI, SRI, mND705, CCRI, and NPCI. These eight indices and FOD_{cb} were used as independent variables, while rice leaf SPAD values were used as the dependent variable, to establish an RF estimation model. To evaluate model performance, the VI_{ss} + FOD_{cb} combination model was compared with models constructed using FOD_{cb} and VI_{ss} alone. The results are shown in Figure 5. As shown in Figure 5, the overall accuracy of the three models decreased in the following order: VI_{ss} + FOD_{cb}-RF > FOD_{cb}-RF > VI_{ss}-RF. The VI_{ss} + FOD_{1.2cb} combined model was the most effective in estimating leaf SPAD values, with calibration set R^2_c and RMSE_c values of 0.977 and 1.460 and validation set R^2_v , RMSE_v, and RPD_v values of 0.821, 2.621, and 2.296, respectively. Compared with the optimal model (FOD_{1.2cb}-RF) constructed using FOD_{cb} alone, the VI_{ss} + FOD_{1.2cb}-RF model showed an improvement of 4.380% in R^2_c , a decrease of 40.481% in RMSE_c, an increase of 1.593% in RPD_v, and a decrease of 2.782% in RMSE_v. Compared with the VI_{ss}-RF model, the VI_{ss} + FOD_{1.2cb}-RF model showed an improvement of 31.141% in R^2_c , a decrease of 70.082% in RMSE_c, an increase of 10.647% in R^2_v , an increase of 44.221% in RPD_v, and a decrease of 16.555% in RMSE_v. In terms of

estimation accuracy for leaf SPAD values, the combined VI_{ss} + FOD_{cb} model demonstrated a notable improvement over the models using FOD_{cb} or VI_{ss} alone. The improvement effect from the model based solely on VI_{ss} was more pronounced than that from the model based solely on FOD_{cb}.

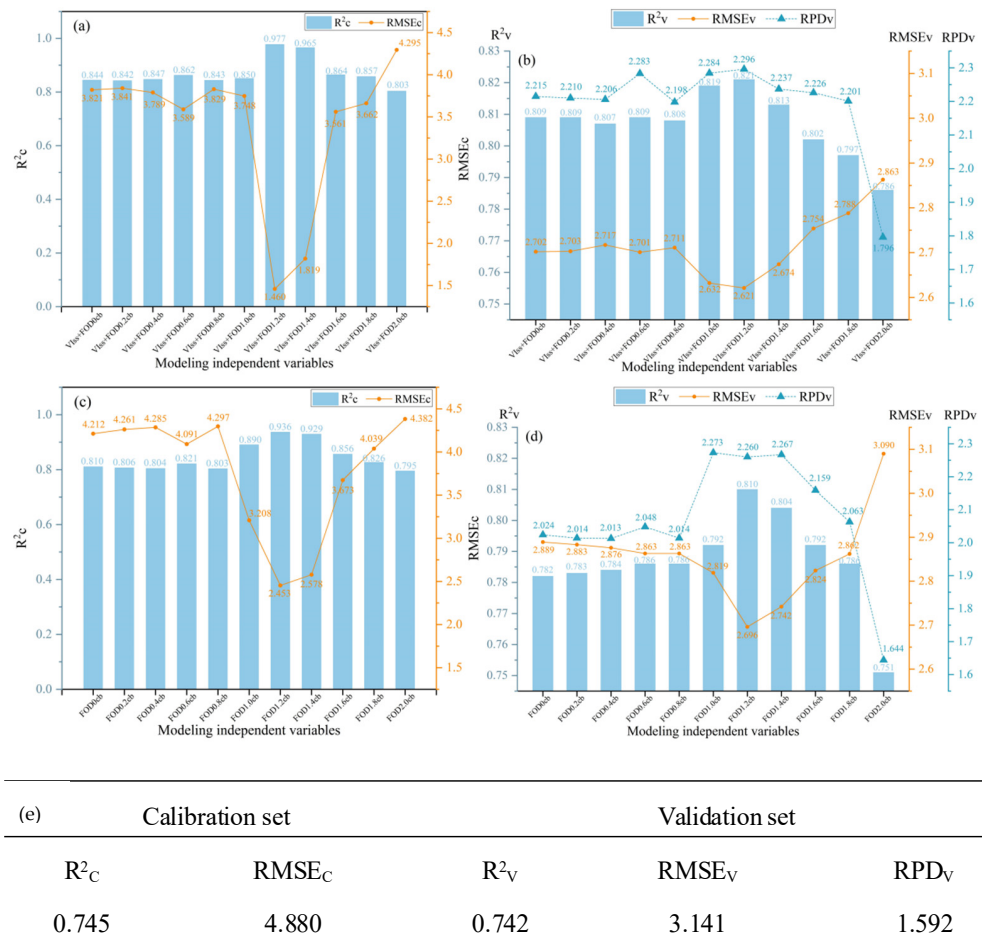


Figure 5. Comparison of modelling accuracy: (a,b) represent the calibration set and validation set of the VI_{ss} + FOD_{cb}-RF model, respectively; (c,d) represent the calibration set and validation set of the FOD_{cb}-RF model, respectively; and (e) represents the results of the VI_{ss}-RF model.

The predicted and observed values of the optimal model based on the combination of VI_{ss} and FOD_{cb}, FOD_{cb} alone, and VI_{ss} alone were linearly fitted, and the results are shown in Figure 6. A regression line closer to the 1:1 line indicates better model quality. Figure 6a–c show that the slopes of the three models were 0.93, 0.90, and 0.68, respectively. The slope of the VI_{ss} + FOD_{1.2cb}-RF model was closest to 1, indicating that this model had the best performance for leaf SPAD values under Cd contamination. However, it is worth noting that the model based on the VI_{ss} alone had a validation set R^2_v greater than 0.7 and an RPD_v greater than 1.5, which allowed for a rough estimation of leaf SPAD values. Nevertheless, as shown in Figure 6c, it can be observed that the VI_{ss}-RF model predicted a large number of data points with the same value, and most of the data points were distributed outside the 95% confidence interval. This further confirms that it is difficult to achieve an effective estimation of leaf SPAD values with a model constructed from vegetation indices that contain limited spectral band information.

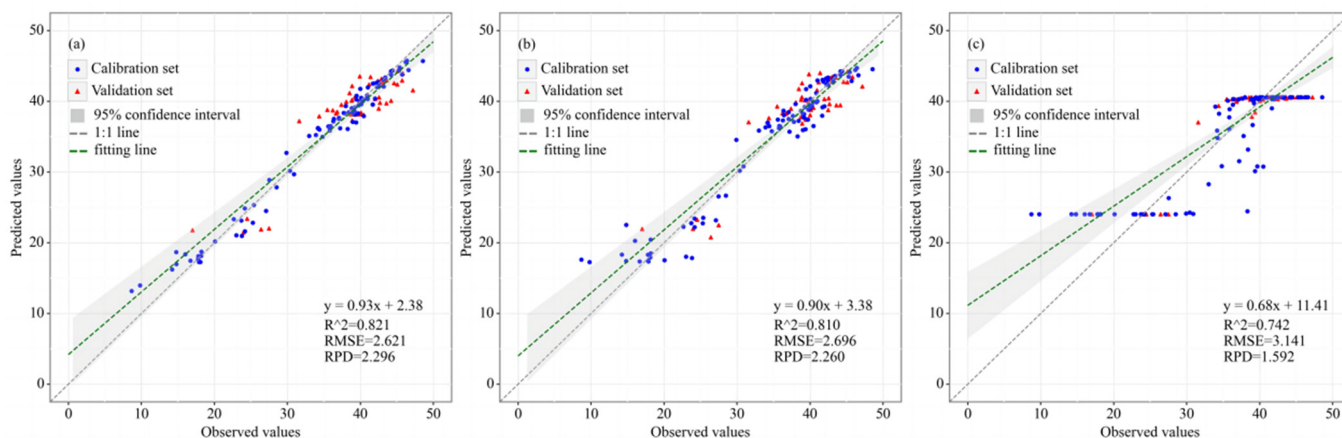


Figure 6. Regression results of the predicted and observed SPAD values based on the optimal models: (a) VI_{SS} + FOD_{1.2cb}-RF, (b) FOD_{1.2cb}-RF, and (c) VI_{SS}-RF.

3.4. Variable Importance of the VI_{SS} + FOD_{cb} Model

To further explain why the modelling performance of the combined VI_{SS} + FOD_{cb} model was better than that of the independent FOD_{cb} and VI_{SS} t models, the importance of the variables in the VI_{SS} + FOD_{cb}-RF model was analyzed. Table 5 shows the independent variables with the top 10 Gini coefficients in the VI_{SS} + FOD_{cb}-RF model. As shown in Table 5, both VI_{SS} and FOD_{cb} played important roles in the combined model. Prior to the 0.6th order, the combination model relied mainly on VI_{SS} for modelling, with only three characteristic bands significantly influencing the model. After the 0.8th order, the number of important characteristic bands in the combination model increased, with the optimal model VI_{SS} + FOD_{1.2cb}-RF having the highest number of important characteristic bands. A total of seven important bands were identified, which were roughly distributed around the 520 nm, 680 nm, and 700 nm bands. Among them, 521 nm and 686 nm were the top two independent variables in the VI_{SS} + FOD_{1.2cb} combined model. This result is consistent with the findings of Liu et al. [75], who identified the 518 nm and 686 nm as key characteristics for estimation of canopy SPAD values in rice at different growth stages. Compared with other combination models, the largest Gini coefficient in the optimal model VI_{SS} + FOD_{1.2cb}-RF corresponded to the spectral characteristic band rather than the VI_{SS}. This suggests that spectral characteristic bands were more important than VIs in the combined model. This further confirms that VIs, which contain limited spectral information, have lower accuracy for estimating SPAD values and that a broader set of spectral characteristic bands should be considered.

Table 5. Top 10 independent variables of the Gini coefficient in the combination model.

Combination Model	Independent Variables
VI _{SS} + FOD _{0cb}	HCSI, SIPI, NDRE, SRI, NDVI, mND705, CCRI, 656 nm, 654 nm, 655 nm
VI _{SS} + FOD _{0.2cb}	HCSI, NDRE, SIPI, SRI, NDVI, mND705, CCRI, 457 nm, 446 nm, 488 nm
VI _{SS} + FOD _{0.4cb}	HCSI, SIPI, NDRE, SRI, NDVI, mND705, 423 nm, CCRI, 424 nm, 419 nm
VI _{SS} + FOD _{0.6cb}	HCSI, SIPI, NDRE, NDVI, 423 nm, SRI, mND705, CCRI, 646 nm, 650 nm
VI _{SS} + FOD _{0.8cb}	HCSI, NDRE, SIPI, SRI, NDVI, mND705, 461 nm, 679 nm, 680 nm, 486 nm
VI _{SS} + FOD _{1.0cb}	SIPI, HCSI, SRI, 756 nm, NDRE, NDVI, 539 nm, 759 nm, 737 nm, 752 nm
VI _{SS} + FOD _{1.2cb}	521 nm, 686 nm, CCRI, SIPI, 520 nm, 703 nm, 685 nm, 515 nm, 687 nm, HCSI
VI _{SS} + FOD _{1.4cb}	CCRI, 686 nm, SIPI, 515 nm, 685 nm, 520 nm, 700 nm, 701 nm, HCSI, SRI
VI _{SS} + FOD _{1.6cb}	HCSI, SIPI, 503 nm, 696 nm, 616 nm, NDVI, NDRE, 697 nm, SRI, mND705
VI _{SS} + FOD _{1.8cb}	HCSI, NDVI, SIPI, NDRE, 509 nm, SRI, 514 nm, 503 nm, 696 nm, 694 nm
VI _{SS} + FOD _{2.0cb}	HCSI, 741 nm, 703 nm, CCRI, SRI, 683 nm, NDVI, 708 nm, SIPI, mND705

4. Discussion

4.1. Spectral Reflectance Changes in Rice Leaves Under Different Scenarios

In this study, we initially investigated the changes in the spectral reflectivity of rice leaves under three different Cd contamination scenarios and found that at visible wavelengths, especially between the “green peaks” and the “red valleys”, the reflectivity in the Cd contamination scenarios was greater than that in the non-Cd-contaminated scenario. This finding is consistent with the study by Chi et al., which revealed that the Cd accumulated in the leaf led to a reduction in chlorophyll concentration, thereby increasing reflectance in the visible spectrum [19]. In addition, this study revealed that the spectral reflectance did not show a clear pattern of change in the near-infrared band range. This finding differs from the results of Chi et al. [19], who suggested that spectral reflectance decreased with increasing Cd concentration in this band range because of the reduction in leaf thickness. This may be because the Cd concentration gradient used in this study was not significantly different, and the treatment concentration was more consistent with that of real Cd-contaminated farmland. Furthermore, 12 rice lines with low Cd accumulation were used in this study following radiation mutagenesis, and the test material may have exhibited some tolerance to Cd. This made it challenging to observe a clear pattern of change in spectral reflectance with Cd treatment. To better understand the effects of Cd stress on the reflectance spectra of rice leaves, future experiments should refine the agronomic setup by incorporating a broader range of Cd treatment levels and diverse rice varieties (low Cd accumulation, high Cd accumulation, and conventional varieties). Moreover, when the spectral data were collected, leaf samples were synchronously gathered for scanning electron microscopy analysis in the laboratory to investigate the underlying mechanism of the spectral response to Cd contamination at the microscopic level.

4.2. Spectral Response Characteristic Bands of Leaf SPAD Values

In this study, the VIP method was applied to select spectral characteristic bands for predicting leaf SPAD values. As demonstrated in Section 3.2, where characteristic bands corresponding to leaf SPAD values were extracted under various FOD transformations, the wavelength range of 400–773 nm was consistently identified across most fractional orders. Therefore, we concluded that the 400–773 nm wavelength range within the visible spectrum was a sensitive area for spectral estimation of leaf SPAD values under Cd contamination. This is primarily due to the fact that reflectance in the visible spectrum is governed by leaf pigments, whereas reflectance in the near-infrared region is more strongly influenced by the structural characteristics of leaf cells. As Cd concentration accumulates in the leaves, leading to a reduction in chlorophyll content, reflectance in the visible range increases, while reflectance in the near-infrared range decreases [19]. Consequently, fluctuations in Cd concentration result in changes to chlorophyll content, which in turn affect the spectral reflectance response across the visible to near-infrared spectrum. This observation further supports the notion that the 400–773 nm wavelength range serves as a characteristic band for assessing SPAD values in Cd-contaminated rice leaves. Furthermore, this finding is consistent with the conclusion of Liu et al., who demonstrated that spectral indices derived from reflectance at 550 nm, 670 nm, 700 nm, 712 nm, and 800 nm can be used to estimate chlorophyll content in rice under Cu and Cd heavy metal contamination [76]. Although VIP methods are often used to select characteristic bands for agronomic parameters [77–79] and soil chemical properties [23,80–82], differences exist in the characteristic bands obtained through different feature selection methods. Methods such as correlation analysis (CA), competitive adaptive reweighted sampling (CARS), the successive projections algorithm (SPA), and uninformative variable elimination (UVE) have also been applied in feature selection [83–85]. In this study, only one commonly used feature selection method was tested.

The impact of different feature selection methods on the stability of spectral characteristic bands warrants further investigation.

4.3. Performance Improvement by the Combined Model

In this paper, we found that the RF model constructed using the combination of VI_{ss} and FOD_{1,2cb} had the best estimation performance for SPAD values. The estimation accuracy of SPAD values was ranked as follows: VI_{ss} + FOD_{cb}-RF > FOD_{cb}-RF > VI_{ss}-RF. This result is consistent with the findings of Feng et al. [86], who reported that the model using characteristic bands as inputs outperformed the model using vegetation indices for the inversion of leaf nitrogen content in japonica rice, and Xu et al. [87], who found that a model combining vegetation indices and textural features was more accurate than a vegetation-indices-only model for estimating aboveground biomass in rice. By analyzing the importance of the modeling variables in the combined model, we found that both VI_{ss} and FOD_{cb} played key roles in the RF modelling process (with Gini coefficients ranked in the top 10). This further confirmed that combining vegetation indices with spectral characteristic bands can improve model accuracy. This improvement is likely due to the fact that vegetation indices, derived from mathematical operations on specific spectral bands, reflect variations in the physiological and biochemical properties of crops to some extent. In contrast, FOD transformations enhance spectral details under heavy metal stress, and the selected characteristic bands contain more spectral information correlated with leaf SPAD values. Consequently, the combined model considers both the broad spectral characteristics indicated by VIs and the detailed features revealed by the FOD_{cb}. Integrating these two aspects helps optimize feature selection, eliminate redundant information, and ultimately enhance the precision of the estimation model. However, this study used only the RF model to compare the estimation performance of the three types of independent variables for leaf SPAD values, without investigating how the models themselves influence estimation accuracy. In future work, a comparative study between linear models and machine-learning models would be valuable.

4.4. Limitations and Research Programs

Leaf SPAD values are key indicators for assessing the health status of crops and the degree of environmental stress. In this paper, a new method for estimating leaf SPAD values, which combines VI_{ss} and FOD_{cb}, is proposed. This method not only improved the accuracy of leaf SPAD value estimation but enabled remote sensing monitoring of the Cd stress effect on rice. In conclusion, the SPAD estimation model proposed in this study was based on data obtained from an artificially controlled Cd pool test. By focusing on a single influencing factor and effectively mitigating the impact of other variables on rice growth, the model demonstrated improved accuracy and stability. However, real-world agricultural fields often experience the coexistence of multiple stresses, such as heavy metals, diseases, insect pests, and drought, which could cause spectral interference. Therefore, a key direction for future research when applying this model in agricultural practice is to develop a method for eliminating the influence of other factors and accurately identifying the Cd stress signals. In addition, this study achieved only ground estimation of leaf SPAD values, and accurate large-scale monitoring requires further research. The integration of multisource remote sensing imagery [48], the construction of satellite-ground spectral correlation transformation relationships [49], and the introduction of environmental factors may provide worthwhile breakthroughs for large-scale and accurate monitoring of Cd stress effects in rice.

5. Conclusions

Compared with the commonly used pot experiments, this study innovatively designed a controlled Cd pool experiment that was more in line with the real growing environment of rice. Based on this experiment, a set of leaf SPAD values and full-spectrum spectral reflectance data under Cd-contaminated conditions covering the entire rice growth period was obtained. In addition, with the help of the FOD and VIP methods, this study accurately identified the characteristic bands of leaf SPAD values from the full-spectrum reflectance spectral information, which addressed the issue of spectral information loss that has occurred in the past when relying solely on vegetation indices. Furthermore, this study proposed a new model combining VI_{ss} and FOD_{cb}, increasing estimation accuracy by 10.65%, reaching over 82% compared with the traditional model based solely on vegetation indices. This indicates that the new model has significant potential for widespread application. In conclusion, this study provides methodological support for the large-scale application of hyperspectral remote sensing in research on rice Cd stress and other adverse physiological conditions.

Author Contributions: Conceptualization, R.T. and B.Z. (Bin Zou); methodology, R.T., H.T. and B.Z. (Bo Zhang); software, R.T.; validation, J.Z. and L.Z.; formal analysis, L.D.; investigation, R.T. and B.Z. (Bo Zhang); resources, S.L. and L.D.; data curation, R.T. and B.Z. (Bin Zou); writing—original draft preparation, R.T.; writing—review and editing, R.T., B.Z. (Bin Zou) and S.L.; visualization, R.T.; supervision, Y.W.; project administration, S.L.; funding acquisition, B.Z. (Bin Zou). All authors have read and agreed to the published version of the manuscript.

Funding: This research was funded by the National Key Research and Development Program of China, grant number 2022YFD1700105, and the Open Subjects of Dongting Lake Basin Ecological Protection and Restoration Engineering and Technology Innovation Center, Ministry of Natural Resources, grant number 2023019.

Institutional Review Board Statement: Not applicable.

Data Availability Statement: The datasets presented in this article are not readily available because the data are part of an ongoing study. Requests to access the datasets should be directed to the corresponding author of this article.

Conflicts of Interest: The authors declare no conflicts of interest.

References

1. Chen, G.; Du, R.Y.; Wang, X. Genetic Regulation Mechanism of Cadmium Accumulation and Its Utilization in Rice Breeding. *Int. J. Mol. Sci.* **2023**, *24*, 1247. [[CrossRef](#)] [[PubMed](#)]
2. Imran, M.; Hussain, S.; He, L.X.; Ashraf, M.F.; Ihtisham, M.; Warraich, E.A.; Tang, X.R. Molybdenum-Induced Regulation of Antioxidant Defense-Mitigated Cadmium Stress in Aromatic Rice and Improved Crop Growth, Yield, and Quality Traits. *Antioxidants* **2021**, *10*, 838. [[CrossRef](#)] [[PubMed](#)]
3. Chen, J.G.; Zou, W.L.; Meng, L.J.; Fan, X.R.; Xu, G.H.; Ye, G.Y. Advances in the Uptake and Transport Mechanisms and QTLs Mapping of Cadmium in Rice. *Int. J. Mol. Sci.* **2019**, *20*, 3417. [[CrossRef](#)] [[PubMed](#)]
4. Sonobe, R.; Sugimoto, Y.; Kondo, R.; Seki, H.; Sugiyama, E.; Kiriwa, Y.; Suzuki, K. Hyperspectral Wavelength Selection for Estimating Chlorophyll Content of Muskmelon Leaves. *Eur. J. Remote Sens.* **2021**, *54*, 512–523. [[CrossRef](#)]
5. Huang, X.; Guan, H.D.; Bo, L.Y.; Xu, Z.Q.; Mao, X.M. Hyperspectral Proximal Sensing of Leaf Chlorophyll Content of Spring Maize Based on A Hybrid of Physically Based Modelling and Ensemble Stacking. *Comput. Electron. Agric.* **2023**, *208*, 107745. [[CrossRef](#)]
6. Sun, J.H.; Yang, L.; Yang, X.T.; Wei, J.; Li, L.T.; Guo, E.H.; Kong, Y.H. Using Spectral Reflectance to Estimate the Leaf Chlorophyll Content of Maize Inoculated With Arbuscular Mycorrhizal Fungi Under Water Stress. *Front. Plant Sci.* **2021**, *12*, 646173. [[CrossRef](#)]
7. Guan, L.; Liu, X.N.; Cheng, C.Q. Research on Hyperspectral Information Parameters of Chlorophyll Content of Rice Leaf in Cd-Polluted Soil Environment. *Spectrosc. Spectr. Anal.* **2009**, *29*, 2713–2716. [[CrossRef](#)]
8. Wu, C.Y.; Liu, M.L.; Liu, X.N.; Wang, T.J.; Wang, L.Y. Developing a new spectral index for detecting cadmium-induced stress in rice on a regional scale. *Int. J. Environ. Res. Public Health* **2019**, *16*, 4811. [[CrossRef](#)]

9. Azia, F.; Stewart, K.A. Relationships Between Extractable Chlorophyll and SPAD Values in Muskmelon Leaves. *J. Plant Nutr.* **2001**, *24*, 961–966. [[CrossRef](#)]
10. Wakiyama, Y. The Relationship between SPAD Values and Leaf Blade Chlorophyll Content throughout the Rice Development Cycle. *JARQ Jpn. Agric. Res. Q.* **2016**, *50*, 329–334. [[CrossRef](#)]
11. Kumar, P.; Sharma, R.K. Development of SPAD Value-Based Linear Models for Non-destructive Estimation of Photosynthetic Pigments in Wheat (*Triticum aestivum* L.). *Indian J. Genet. Plant Breed.* **2019**, *79*, 96–99. [[CrossRef](#)]
12. Yang, Y.C.; Nan, R.; Mi, T.X.; Song, Y.X.; Shi, F.H.; Liu, X.R.; Wang, Y.Q.; Sun, F.L.; Xi, Y.J.; Zhang, C. Rapid and Nondestructive Evaluation of Wheat Chlorophyll under Drought Stress Using Hyperspectral Imaging. *Int. J. Mol. Sci.* **2023**, *24*, 5825. [[CrossRef](#)] [[PubMed](#)]
13. El-Hendawy, S.; Dewir, Y.H.; Elsayed, S.; Schmidhalter, U.; Al-Gaadi, K.; Tola, E.; Refay, Y.; Tahir, M.U.; Hassan, W.M. Combining Hyperspectral Reflectance Indices and Multivariate Analysis to Estimate Different Units of Chlorophyll Content of Spring Wheat under Salinity Conditions. *Plants* **2022**, *11*, 456. [[CrossRef](#)] [[PubMed](#)]
14. Yao, Z.F.; Lei, Y.; He, D.J. Early visual detection of wheat stripe rust using visible/near-infrared hyperspectral imaging. *Sensors* **2019**, *19*, 952. [[CrossRef](#)]
15. Wang, H.F.; Huo, Z.G.; Zhou, G.S.; Liao, Q.H.; Feng, H.K.; Wu, L. Estimating Leaf SPAD Values of Freeze-damaged Winter Wheat using Continuous Wavelet Analysis. *Plant Physiol. Biochem.* **2016**, *98*, 39–45. [[CrossRef](#)]
16. Yuan, X.T.; Zhang, X.; Zhang, N.N.; Ma, R.; He, D.D.; Bao, H.; Sun, W.J. Hyperspectral Estimation of SPAD Value of Cotton Leaves under Verticillium Wilt Stress Based on GWO—ELM. *Agriculture* **2023**, *13*, 1779. [[CrossRef](#)]
17. Cao, Y.F.; Xu, H.L.; Song, J.; Yang, Y.; Hu, X.H.; Wiyao, K.T.; Zhai, Z.Y. Applying Spectral Fractal Dimension Index to Predict the SPAD Value of Rice Leaves under Bacterial Blight Disease Stress. *Plant Methods.* **2022**, *18*, 67. [[CrossRef](#)]
18. Priya, S.; Ghosh, R. Monitoring Effects of Heavy Metal Stress on Biochemical and Spectral Parameters of Cotton using Hyperspectral Reflectance. *Environ. Monit. Assess.* **2023**, *195*, 112. [[CrossRef](#)] [[PubMed](#)]
19. Chi, G.Y.; Huang, B.; Chen, X.; Shi, Y.; Zheng, T.H. Effects of Cadmium on Visible and Near-infrared Reflectance Spectra of Rice (*Oryza sativa* L.). *Fresenius Environ. Bull.* **2011**, *20*, 391–397.
20. Zhang, J.H.; Zeng, L.S.; Sun, Y.H.; Song, C.Y.; Wang, H.; Chen, J.M.; Biradar, C. A pilot study on the effect of Cu, Zn, and Cd on the spectral curves and chlorophyll of wheat canopy at tiller stage. *Toxicol. Environ. Chem.* **2015**, *97*, 454–463. [[CrossRef](#)]
21. Li, Y.X.; Chen, X.Y.; Luo, D.; Li, B.Y.; Wang, S.R.; Zhang, L.W. Effects of Cuprum Stress on Position of Red Edge of Maize Leaf Reflection Hyperspectra and Relations to Chlorophyll Content. *Spectrosc. Spectr. Anal.* **2018**, *38*, 546–551.
22. Zhou, L.; Zhou, L.J.Y.; Wu, H.B.; Kong, L.J.; Li, J.S.; Qiao, J.L.; Chen, L.M. Analysis of Cadmium Contamination in Lettuce (*Lactuca sativa* L.) Using Visible-Near Infrared Reflectance Spectroscopy. *Sensors* **2023**, *23*, 9562. [[CrossRef](#)] [[PubMed](#)]
23. Tu, Y.L.; Zou, B.; Feng, H.H.; Zhou, M.; Yang, Z.H.; Xiong, Y. A Near Standard Soil Samples Spectra Enhanced Modeling Strategy for Cd Concentration Prediction. *Remote Sens.* **2021**, *13*, 2657. [[CrossRef](#)]
24. Zou, B.; Jiang, X.L.; Feng, H.H.; Tu, Y.L.; Tao, C. Multisource spectral-integrated estimation of cadmium concentrations in soil using a direct standardization and Spiking algorithm. *Sci. Total Environ.* **2020**, *701*, 134890. [[CrossRef](#)] [[PubMed](#)]
25. Wang, Y.L.; Zou, B.; Chai, L.Y.; Lin, Z.; Feng, H.H.; Tang, Y.Q.; Tian, R.C.; Tu, Y.L.; Zhang, B.; Zou, H.J. Monitoring of soil heavy metals based on hyperspectral remote sensing: A review. *Earth-Sci. Rev.* **2024**, *254*, 104814. [[CrossRef](#)]
26. Zhang, S.; Fei, T.; Chen, Y.; Hong, Y. Estimating Cadmium-lead Concentrations in Rice Blades through Fractional Order Derivatives of Foliar Spectra. *Biosyst. Eng.* **2022**, *219*, 177–188. [[CrossRef](#)]
27. Wang, X.P.; Zhang, F.; Kung, H.T.; Johnson, V.C. New Methods for Improving the Remote Sensing Estimation of Soil Organic Matter Content (SOMC) in the Ebinur Lake Wetland National Nature Reserve (ELWNNR) in Northwest China. *Remote Sens. Environ.* **2018**, *218*, 104–118. [[CrossRef](#)]
28. Geng, J.; Lv, J.; Pei, J.; Liao, C.; Tan, Q.; Wang, T.; Fang, H.; Wang, L. Prediction of Soil Organic Carbon in Black Soil Based on A Synergistic Scheme from Hyperspectral Data: Combining fractional-order derivatives and three-dimensional spectral indices. *Comput. Electron. Agric.* **2024**, *220*, 108905. [[CrossRef](#)]
29. Hong, Y.; Guo, L.; Chen, S.; Linderman, M.; Mouazen, A.M.; Yu, L.; Chen, Y.; Liu, Y.; Liu, Y.; Cheng, H.; et al. Exploring the Potential of Airborne Hyperspectral Image for Estimating Topsoil Organic Carbon: Effects of Fractional-order Derivative and Optimal Band Combination Algorithm. *Geoderma* **2020**, *365*, 114228. [[CrossRef](#)]
30. Jin, H.; Peng, J.; Bi, R.; Tian, H.; Zhu, H.; Ding, H. Comparing Laboratory and Satellite Hyperspectral Predictions of Soil Organic Carbon in Farmland. *Agronomy* **2024**, *14*, 175. [[CrossRef](#)]
31. Meng, X.; Bao, Y.; Ye, Q.; Liu, H.; Zhang, X.; Tang, H.; Zhang, X. Soil Organic Matter Prediction Model with Satellite Hyperspectral Image Based on Optimized Denoising Method. *Remote Sens.* **2021**, *13*, 2273. [[CrossRef](#)]
32. Chen, L.; Lai, J.; Tan, K.; Wang, X.; Chen, Y.; Ding, J. Development of A Soil Heavy Metal Estimation Method Based on A Spectral Index: Combining Fractional-order Derivative Pretreatment and the Absorption Mechanism. *Sci. Total Environ.* **2022**, *813*, 151882. [[CrossRef](#)] [[PubMed](#)]

33. Cui, S.; Zhou, K.; Ding, R.; Cheng, Y.; Jiang, G. Estimation of Soil Copper Content Based on Fractional-order Derivative Spectroscopy and Spectral Characteristic Band Selection. *Spectrosc. Acta Part A Mol. Biomol. Spectrosc.* **2022**, *275*, 121190. [[CrossRef](#)] [[PubMed](#)]
34. Wang, Z.; Zhang, X.L.; Zhang, F.; Chan, N.W.; Kung, H.T.; Liu, S.H.; Deng, L.F. Estimation of Soil Salt Content using Machine Learning Techniques Based on Remote-sensing Fractional Derivatives, A Case Study in the Ebinur Lake Wetland National Nature Reserve, Northwest China. *Ecol. Indic.* **2020**, *119*, 106869. [[CrossRef](#)]
35. Fu, C.; Tian, A.; Zhu, D.; Zhao, J.; Xiong, H. Estimation of Salinity Content in Different Saline-Alkali Zones Based on Machine Learning Model Using FOD Pretreatment Method. *Remote Sens.* **2021**, *13*, 5140. [[CrossRef](#)]
36. Zhang, D.; Tiyip, T.; Ding, J.; Zhang, F.; Nurmemet, I.; Kelimu, A.; Wang, J. Quantitative Estimating Salt Content of Saline Soil Using Laboratory Hyperspectral Data Treated by Fractional Derivative. *J. Spectrosc.* **2016**, *2016*, 1081674. [[CrossRef](#)]
37. Ning, J.; Zou, B.; Tu, Y.L.; Zhang, X.; Wang, Y.L.; Tian, R.C. Evaluation of Soil As Concentration Estimation Method Based on Spectral Indices. *Spectrosc. Spectr. Anal.* **2024**, *44*, 1472–1481.
38. Soil environmental quality Risk control standard for soil contamination of agricultural land. *GB15618-2018*; Ministry of Ecology and Environment: Beijing, China, 2018.
39. Zhang, B.; Ye, W.J.; Ren, D.Y.; Tian, P.; Peng, Y.L.; Gao, Y.; Ruan, B.P.; Wang, L.; Zhang, G.H.; Guo, L.B.; et al. Genetic Analysis of Flag Leaf Size and Candidate Genes Determination of A Major QTL for Flag Leaf Width in Rice. *Rice* **2015**, *8*, 2. [[CrossRef](#)] [[PubMed](#)]
40. Hu, C.Y.; Rao, J.; Song, Y.; Chan, S.A.; Tohge, T.; Cui, B.; Lin, H.; Fernie, A.R.; Zhang, D.B.; Shi, J.X. Dissection of Flag Leaf Metabolic Shifts and their Relationship with those Occurring Simultaneously in Developing Seed by Application of Non-targeted Metabolomics. *PLoS ONE* **2020**, *15*, e0227577. [[CrossRef](#)] [[PubMed](#)]
41. Wang, L.; Chen, S.S.; Peng, Z.P.; Huang, J.C.; Wang, C.Y.; Jiang, H.; Zheng, Q.; Li, D. Phenology Effects on Physically Based Estimation of Paddy Rice Canopy Traits from UAV Hyperspectral Imagery. *Remote Sens.* **2021**, *13*, 1792. [[CrossRef](#)]
42. Feng, H.; Chen, G.X.; Xiong, L.Z.; Liu, Q.; Yang, W.N. Accurate Digitization of the Chlorophyll Distribution of Individual Rice Leaves using Hyperspectral Imaging and An Integrated Image Analysis Pipeline. *Front. Plant Sci.* **2017**, *8*, 1238. [[CrossRef](#)] [[PubMed](#)]
43. Yue, J.B.; Wang, J.; Zhang, Z.Y.; Li, C.C.; Yang, H.; Feng, H.K.; Guo, W. Estimating Crop Leaf Area Index and Chlorophyll Content using A Deep Learning-based Hyperspectral Analysis Method. *Comput. Electron. Agric.* **2024**, *227*, 109653. [[CrossRef](#)]
44. Wen, S.Y.; Shi, N.; Lu, J.W.; Gao, Q.W.; Hu, W.R.; Cao, Z.D.; Lu, J.X.; Yang, H.B.; Gao, Z.Q. Continuous Wavelet Transform and Back Propagation Neural Network for Condition Monitoring Chlorophyll Fluorescence Parameters Fv/Fm of Rice Leaves. *Agriculture* **2022**, *12*, 1197. [[CrossRef](#)]
45. Zhang, J.; Guo, Z.; Ren, Z.S.; Wang, S.H.; Yue, M.H.; Zhang, S.S.; Yin, X.; Gong, K.J.; Ma, C.Y. Rapid Determination of Protein, Starch and Moisture Content in Wheat Flour by Near-Infrared Hyperspectral Imaging. *J. Food Compos. Anal.* **2023**, *117*, 105134. [[CrossRef](#)]
46. Caporaso, N.; Whitworth, M.B.; Fisk, I.D. Near-Infrared Spectroscopy and Hyperspectral Imaging for Non-Destructive Quality Assessment of Cereal Grains. *Appl. Spectrosc. Rev.* **2018**, *53*, 667–687. [[CrossRef](#)]
47. Aulia, R.; Kim, Y.; Amanah, H.Z.; Andi, A.M.A.; Kim, H.; Kim, H.; Lee, W.H.; Kim, K.H.; Baek, J.H.; Cho, B.K. Non-Destructive Prediction of Protein Contents of Soybean Seeds using Near-Infrared Hyperspectral Imaging. *Infrared Phys. Technol.* **2022**, *127*, 104365. [[CrossRef](#)]
48. He, Z.H.; Ma, Z.H.; Li, M.C.; Zhou, Y. Selection of A Calibration Sample Subset by A Semi-supervised Method. *J. Near Infrared Spectrosc.* **2018**, *26*, 87–94. [[CrossRef](#)]
49. Li, H.; Wang, J.X.; Xing, Z.N.; Shen, G. Influence of Improved Kennard/Stone Algorithm on the Calibration Transfer in Near-Infrared Spectroscopy. *Spectrosc. Spectr. Anal.* **2011**, *31*, 362–365. [[CrossRef](#)]
50. Zhou, X.; Huang, W.; Zhang, J.; Kong, W.; Casa, R.; Huang, Y. A Novel Combined Spectral Index for Estimating the Ratio of Carotenoid to Chlorophyll Content to Monitor Crop Physiological and Phenological Status. *Int. J. Appl. Earth Obs. Geoinf.* **2019**, *76*, 128–142. [[CrossRef](#)]
51. Aparicio, N.; Villegas, D.; Royo, C.; Casadesus, J.; Araus, J.L. Effect of Sensor View Angle on the Assessment of Agronomic Traits by Ground Level Hyper-spectral Reflectance Measurements in Durum Wheat under Contrasting Mediterranean Conditions. *Int. J. Remote Sens.* **2004**, *25*, 1131–1152. [[CrossRef](#)]
52. Sims, D.A.; Gamon, J. A Relationships between Leaf Pigment Content and Spectral Reflectance Across a Wide Range of Species, Leaf Structures and Developmental Stages. *Remote Sens. Environ.* **2002**, *81*, 337–354. [[CrossRef](#)]
53. Liu, N.; Townsend, P.A.; Naber, M.R.; Bethke, P.C.; Hills, W.B.; Wang, Y. Hyperspectral Imagery to Monitor Crop Nutrient Status Within and Across Growing Seasons. *Remote Sens. Environ.* **2021**, *255*, 112303. [[CrossRef](#)]
54. Peñuelas, J.; Gamon, J.; Fredeen, A.; Merino, J.; Field, C. Reflectance Indices Associated with Physiological Changes in Nitrogen and Water-limited Sunflower Leaves. *Remote Sens. Environ.* **1994**, *48*, 135–146. [[CrossRef](#)]

55. Barnes, J.D.; Balaguer, L.; Manrique, E.; Elvira, S.; Davison, A. A Reappraisal of the Use of DMSO for the Extraction and Determination of Chlorophylls A and B in Lichens and Higher Plants. *Environ. Exp. Bot.* **1992**, *32*, 85–100. [[CrossRef](#)]
56. Penuelas, J.; Baret, F.; Filella, I. Semi-empirical Indices to Assess Carotenoids/Chlorophyll A Ratio from Leaf Spectral Reflectance. *Photosynthetica* **1995**, *31*, 221–230.
57. Daughtry, C.S.; Walthall, C.; Kim, M.; De Colstoun, E.B.; McMurtrey Iii, J. Estimating Corn Leaf Chlorophyll Concentration from Leaf and Canopy Reflectance. *Remote Sens. Environ.* **2000**, *74*, 229–239. [[CrossRef](#)]
58. Haboudane, D.; Miller, J.R.; Tremblay, N.; Zarco-Tejada, P.J.; Dextraze, L. Integrated Narrow-band Vegetation Indices for Prediction of Crop Chlorophyll Content for Application to Precision Agriculture. *Remote Sens. Environ.* **2002**, *81*, 416–426. [[CrossRef](#)]
59. Li, X.Q.; Liu, X.N.; Liu, M.L.; Wang, C.C.; Xia, X.P. A hyperspectral index sensitive to subtle changes in the canopy chlorophyll content under arsenic stress. *Int. J. Appl. Earth Obs. Geoinf.* **2015**, *36*, 41–53. [[CrossRef](#)]
60. Gitelson, A.A.; Gritz, Y.; Merzlyak, M.N. Relationships between Leaf Chlorophyll Content and Spectral Reflectance and Algorithms for Non-destructive Chlorophyll Assessment in Higher Plant Leaves. *J. Plant Physiol.* **2003**, *160*, 271–282. [[CrossRef](#)]
61. Barnes, E.; Clarke, T.; Richards, S.; Colaizzi, P.; Haberland, J.; Kostrzewski, M.; Waller, P.; Choi, C.; Riley, E.; Thompson, T. Coincident Detection of Crop Water Stress, Nitrogen Status and Canopy Density using Ground Based Multispectral Data. In Proceedings of the 5th International Conference on Precision Agriculture, Bloomington, MN, USA, 16 July 2000.
62. Zhang, A.W.; Yin, S.N.; Wang, J.; He, N.P.; Chai, S.T.; Pang, H.Y. Grassland Chlorophyll Content Estimation from Drone Hyperspectral Images Combined with Fractional-Order Derivative. *Remote Sens.* **2023**, *15*, 5623. [[CrossRef](#)]
63. Chong, I.G.; Jun, C.H. Performance of Some Variable Selection Methods When Multicollinearity is Present. *Chemom. Intell. Lab. Syst.* **2005**, *78*, 103–112. [[CrossRef](#)]
64. Wang, Y.T.; Zhan, Y.G.; Yan, G.J.; Xie, D.H. Generalized Fine-Resolution FPAR Estimation using Google Earth Engine: Random Forest or Multiple Linear Regression. *IEEE J. Sel. Top. Appl. Earth Observ. Remote Sens.* **2022**, *16*, 918–929. [[CrossRef](#)]
65. Wang, X.R.; Zhang, C.; Qiang, Z.P.; Xu, W.H.; Fan, J.M. A New Forest Growing Stock Volume Estimation Model Based on AdaBoost and Random Forest Model. *Forests* **2024**, *15*, 260. [[CrossRef](#)]
66. Li, X.Y.; Jin, H.X.; Eklundh, L.; Bouras, E.H.; Olsson, P.O.; Cai, Z.Z.; Ardö, J.; Duan, Z. Estimation of District-level Spring Barley Yield in Southern Sweden using Multi-source Satellite Data and Random Forest Approach. *Int. J. Appl. Earth Obs. Geoinf.* **2024**, *134*, 104183. [[CrossRef](#)]
67. Wang, S.; Tuya, H.; Zhang, S.W.; Zhao, X.Y.; Liu, Z.Q.; Li, R.S.; Lin, X. Random Forest Method for Analysis of Remote Sensing Inversion of Aboveground Biomass and Grazing Intensity of Grasslands in Inner Mongolia, China. *Int. J. Remote Sens.* **2023**, *44*, 2867–2884. [[CrossRef](#)]
68. Yang, H.B.; Li, F.; Wang, W.; Yu, K. Estimating Above-Ground Biomass of Potato Using Random Forest and Optimized Hyperspectral Indices. *Remote Sens.* **2021**, *13*, 2339. [[CrossRef](#)]
69. Shah, S.H.; Angel, Y.; Houborg, R.; Ali, S.; McCabe, M.F. A Random Forest Machine Learning Approach for the Retrieval of Leaf Chlorophyll Content in Wheat. *Remote Sens.* **2019**, *11*, 920. [[CrossRef](#)]
70. López-Calderón, M.J.; Estrada-Avalos, J.; Rodríguez-Moreno, V.M.; Mauricio-Ruvalcaba, J.E.; Martínez-Sifuentes, A.R.; Delgado-Ramírez, G.; Miguel-Valle, E. Estimation of Total Nitrogen Content in Forage Maize (*Zea mays* L.) Using Spectral Indices: Analysis by Random Forest. *Agriculture* **2020**, *10*, 451. [[CrossRef](#)]
71. Wang, C.Y.; Gao, B.B.; Yang, K.; Wang, Y.X.; Sukhbaatar, C.; Yin, Y.; Feng, Q.L.; Yao, X.C.; Zhang, Z.H.; Yang, J.Y. Inversion of Soil Organic Carbon Content Based on the Two-point Machine Learning Method. *Sci. Total Environ.* **2024**, *943*, 173608. [[CrossRef](#)] [[PubMed](#)]
72. Fan, L.; Fang, S.B.; Fan, J.L.; Wang, Y.; Zhan, L.Q.; He, Y.K. Rice Yield Estimation Using Machine Learning and Feature Selection in Hilly and Mountainous Chongqing, China. *Agriculture* **2024**, *14*, 1615. [[CrossRef](#)]
73. Lin, N.; Ma, X.H.; Jiang, R.Z.; Wu, M.H.; Zhang, W.C. Estimation of Maize Residue Cover Using Remote Sensing Based on Adaptive Threshold Segmentation and CatBoost Algorithm. *Agriculture* **2024**, *14*, 711. [[CrossRef](#)]
74. Yang, J.X.; Li, X.G.; Ma, X.F. Improving the Accuracy of Soil Organic Carbon Estimation: CWT-Random Frog-XGBoost as a Prerequisite Technique for In Situ Hyperspectral Analysis. *Remote Sens.* **2023**, *15*, 5294. [[CrossRef](#)]
75. Liu, H.H.; Lei, X.Q.; Liang, H.; Wang, X. Multi-model rice canopy chlorophyll content inversion based on UAV hyperspectral images. *Sustainability* **2023**, *15*, 7038. [[CrossRef](#)]
76. Liu, M.L.; Liu, X.N.; Li, M.; Fang, M.H.; Chi, W.X. Neural-network Model for Estimating Leaf Chlorophyll Concentration in Rice Under Stress from Heavy Metals Using Four Spectral Indices. *Biosyst. Eng.* **2010**, *106*, 223–233. [[CrossRef](#)]
77. Wang, X.; Xu, G.; Feng, Y.; Peng, J.; Gao, Y.; Li, J.; Han, Z.; Luo, Q.; Ren, H.; You, X.J.A.; et al. Estimation Model of Rice Aboveground Dry Biomass Based on the Machine Learning and Hyperspectral Characteristic Parameters of the Canopy. *Agronomy* **2023**, *13*, 1940. [[CrossRef](#)]
78. Li, X.; Zhang, Y.; Bao, Y.; Luo, J.; Jin, X.; Xu, X.; Song, X.; Yang, G. Exploring the Best Hyperspectral Features for LAI Estimation using Partial Least Squares Regression. *Remote Sens.* **2014**, *6*, 6221–6241. [[CrossRef](#)]

79. Verma, B.; Prasad, R.; Srivastava, P.K.; Yadav, S.A.; Singh, P.; Singh, R. Investigation of Optimal Vegetation Indices for Retrieval of Leaf Chlorophyll and Leaf Area Index using Enhanced Learning Algorithms. *Comput. Electron. Agric.* **2022**, *192*, 106581. [[CrossRef](#)]
80. Wei, G.F.; Li, Y.; Zhang, Z.T.; Chen, Y.W.; Chen, J.Y.; Yao, Z.H.; Lao, C.C.; Chen, H.F. Estimation of Soil Salt Content by Combining UAV-borne Multispectral Sensor and Machine Learning Algorithms. *PeerJ* **2020**, *8*, e9087. [[CrossRef](#)] [[PubMed](#)]
81. Shi, X.Y.; Song, J.H.; Wang, H.J.; Lv, X.; Zhu, Y.Q.; Zhang, W.X.; Bu, W.Q.; Zeng, L.Y. Improving Soil Organic Matter Estimation Accuracy by Combining Optimal Spectral Preprocessing and Feature Selection Methods Based on PXRF and VIS-NIR Data Fusion. *Geoderma* **2023**, *430*, 116301. [[CrossRef](#)]
82. Sun, W.C.; Liu, S.; Zhang, X.; Li, Y. Estimation of Soil Organic Matter Content using Selected Spectral Subset of Hyperspectral Data. *Geoderma* **2022**, *409*, 115653. [[CrossRef](#)]
83. Bai, Z.J.; Xie, M.D.; Hu, B.F.; Luo, D.F.; Wan, C.; Peng, J.; Shi, Z. Estimation of Soil Organic Carbon Using Vis-NIR Spectral Data and Spectral Feature Bands Selection in Southern Xinjiang, China. *Sensors* **2022**, *22*, 6124. [[CrossRef](#)] [[PubMed](#)]
84. Fan, L.L.; Zhao, J.L.; Xu, X.G.; Liang, D.; Yang, G.J.; Feng, H.K.; Yang, H.; Wang, Y.L.; Chen, G.; Wei, P.F. Hyperspectral-Based Estimation of Leaf Nitrogen Content in Corn Using Optimal Selection of Multiple Spectral Variables. *Sensors* **2019**, *19*, 2898. [[CrossRef](#)]
85. Wu, G.S.; Fang, Y.L.; Jiang, Q.Y.; Cui, M.; Li, N.; Ou, Y.M.; Diao, Z.H.; Zhang, B.H. Early Identification of Strawberry Leaves Disease Utilizing Hyperspectral Imaging Combining with Spectral Features, Multiple Vegetation Indices and Textural Features. *Comput. Electron. Agric.* **2023**, *204*, 107553. [[CrossRef](#)]
86. Feng, S.; Cao, Y.L.; Xu, T.Y.; Yu, F.H.; Chen, C.L.; Zhao, D.X.; Yan, J. Inversion Based on High Spectrum and NSGA2-ELM Algorithm for the Nitrogen Content of Japonica Rice Leaves. *Spectrosc. Spectr. Anal.* **2020**, *40*, 2584–2591.
87. Xu, T.; Wang, F.; Xie, L.; Yao, X.; Zheng, J.; Li, J.; Chen, S. Integrating the Textural and Spectral Information of UAV Hyperspectral Images for the Improved Estimation of Rice Aboveground Biomass. *Remote Sens.* **2022**, *14*, 2534. [[CrossRef](#)]

Disclaimer/Publisher’s Note: The statements, opinions and data contained in all publications are solely those of the individual author(s) and contributor(s) and not of MDPI and/or the editor(s). MDPI and/or the editor(s) disclaim responsibility for any injury to people or property resulting from any ideas, methods, instructions or products referred to in the content.